Correspondence to:
L. A. Parsons,
lakp@uw.edu

Author Contributions:
Conceptualization: L.A. Parsons
Data curation: L.A. Parsons
Formal analysis: L.A. Parsons, G.J. Hakim
Investigation: L.A. Parsons
Project administration: L.A. Parsons, G.J. Hakim
Resources: L.A. Parsons
Supervision: L.A. Parsons, G.J. Hakim
Validation: L.A. Parsons
Visualization: L.A. Parsons
Writing - original draft: L.A. Parsons
Writing – review & editing: L. Parsons, G.J. Hakim

Local Regions Associated With Interdecadal Global Temperature Variability in the Last Millennium Reanalysis and CMIP5 Models

L.A. Parsons[1] ![ID] **and G.J. Hakim[1]** ![ID]

[1]Department of Atmospheric Sciences, University of Washington, Seattle, WA, USA

Abstract Despite the importance of interdecadal climate variability, we have a limited understanding of which geographic regions are associated with global temperature variability at these timescales. The instrumental record tends to be too short to develop sample statistics to study interdecadal climate variability, and Coupled Model Intercomparison Project, Phase 5 (CMIP5) climate models tend to disagree about which locations most strongly influence global mean interdecadal temperature variability. Here we use a new paleoclimate data assimilation product, the Last Millennium Reanalysis (LMR), to examine where local variability is associated with global mean temperature variability at interdecadal timescales. The LMR framework uses an ensemble Kalman filter data assimilation approach to combine the latest paleoclimate data and state-of-the-art model data to generate annually resolved field reconstructions of surface temperature, which allow us to explore the timing and dynamics of preinstrumental climate variability in new ways. The LMR consistently shows that the middle- to high-latitude north Pacific and the high-latitude North Atlantic tend to lead global temperature variability on interdecadal timescales. These findings have important implications for understanding the dynamics of low-frequency climate variability in the preindustrial era.

Plain Language Summary The combined impacts of natural climate variability and global warming will define how we experience 21st century climate change. Despite the importance of climate variability at interdecadal timescales, we have a limited understanding of which regions around the globe may be driving decade-long warming and cooling shifts in global surface air temperature. It is difficult to study temperature variations lasting decades to centuries because instrumental observations are too short, and climate model simulations disagree on regional sources of natural climate variability. Here we use a new data set, the Last Millennium Reanalysis, that combines preinstrumental (paleoclimate) records with climate model data to extend our knowledge of past climate variations and what may be causing them. The Last Millennium Reanalysis data suggest that regions of the North Pacific and North Atlantic Oceans are associated with global temperature variations on decadal timescales.

1. Introduction

In the coming decades, much of the regional impact of global warming will be determined by the combined effects of climate variability superimposed on a warming signal (e.g., Hawkins & Sutton, 2009; Kirtman et al., 2013). Internal climate variability and climate variability driven by natural forcing are important because they can either enhance or mask anthropogenic surface air temperature (SAT) warming in a given geographic region or on a global scale (e.g., Hegerl et al., 2018; Knutson et al., 2016; Meehl et al., 2011, 2013; Schurer et al., 2015; Steinman et al., 2015; Trenberth & Fasullo, 2013; Watanabe et al., 2014). Intradecadal regional- and global-scale temperature variability is relatively well studied (e.g., Jones, 1989; Trenberth et al., 1998), but we have a limited understanding of the drivers of lower frequency climate variability (Masson-Delmotte et al., 2013).

Although much progress has been made characterizing Earth's global and hemispheric-scale temperature response to climate forcings (e.g., Crowley, 2000; Goosse et al., 2005; Schurer et al., 2013), the specific sources of global, interdecadal temperature variability remain poorly constrained. The instrumental record is too short to adequately estimate variability at these timescales, so paleoclimate records and climate model simulations must be used to study this lower frequency climate variability (e.g., Masson-Delmotte et al., 2013). Model simulations are often used to study interdecadal climate variability (e.g., Stolpe et al., 2017, 2018;

Stouffer et al., 2000), but Brown et al. (2016, 2015) show that climate models disagree about which geographic regions may be influencing global mean surface air temperatures (GMSAT) at interdecadal timescales. Paleoclimate data can provide an observation-based perspective of low-frequency climate variability, but proxy records are noisy recorders of climate signals and are unevenly (and sparsely) distributed around the globe.

Here, we take advantage of recent advances in climate modeling, proxy record availability, and data assimilation to generate annually resolved SAT reconstructions of the last millennium (LM) in the Last Millennium Reanalysis (LMR) framework (Hakim et al., 2016; Steiger et al., 2014, 2018; Tardif et al., 2019). We use data assimilation to bring a hybrid proxy-model perspective to the question of which regions are influencing GMSAT. The LMR framework combines the physically-based covariances in climate models with the observationally-based timing of variability in paleoclimate records. This observation-model hybrid is used to advance understanding of the local and regional drivers of preinstrumental climate variability.

To determine which regions may influence low-frequency global temperature variability in models and the LMR, we employ two methods. First, we use a regression-based approach to measure the relationship between local grid point variability and GMSAT variability at interdecadal timescales. Following Brown et al. (2015), we define a location as a "Region of Significant Influence" (ROSI) on GMSAT at interdecadal timescales if the location shows a significant, positive relationship with GMSAT and local variability leads GMSAT, implying that local dynamics may be driving global changes. As we describe in sections 1 and 3, this ROSI method uses GMSAT as the predictor in the regression calculations. Therefore, we also use a spectral coherence method (e.g., Mann & Park, 1993) to find local regions that have a significant relationship with GMSAT and lead GMSAT variability at interdecadal timescales.

The remainder of the paper is structured as follows. Section 2 describes the climate model data, proxy data, LMR framework, and analytical methods. Section 3 describes results of the two analytical methods to determine the regions associated with interdecadal changes in GMSAT. Section 4 presents our conclusions and discusses potential limitations to using paleoclimate reconstructions and the LMR framework to study local air temperature variability.

2. Data and Methods

2.1. CMIP5 LM

We use gridded SAT model output from 10 all-forcing Coupled Model Intercomparison Project, Phase 5 (CMIP5) LM model simulations spanning the years 850–1849 CE (Schmidt et al., 2011; Taylor et al., 2012): BCC-CSM1-1, NCAR-CCSM4, CSIRO-Mk3L-1-2, FGOALS-s2, GISS-E2-R r1i1p121, HadCM3, IPSL-CM5A-LR, MIROC-ESM, MPI-ESM-P, and MRI-CGCM3. Here we limit our analysis to the pre-industrial era to distinguish preanthropogenic, low-frequency temperature variability from the recent global warming signal and to avoid the potential impact of recent warming on natural, internal climate variability (e.g., Brown et al., 2017; Rind et al., 1989; Stouffer & Wetherald, 2007). CMIP5 data are regridded to a standard ~2° × 2° grid (the Twentieth Century Reanalysis grid; Compo et al., 2011) before regression and coherence calculations.

2.2. LMR and Paleoclimate Data Assimilation

CMIP5 models can provide a dynamically consistent, spatially complete picture of variability in the climate system, but the timing of variability in these models may not coincide with the timing of variability in observations. Paleoclimate data can provide an observation-based constraint on the timing of variability as it has occurred in the "real world," but these proxy records tend to be noisy records of the climate and unevenly spaced geographically. The LMR framework uses an ensemble Kalman filter data assimilation approach to combine paleoclimate data and CMIP5 data by accounting for the uncertainty in each. The LMR relies on covariances in climate model data and the timing and magnitude of variability in paleoclimate data to generate annually resolved field reconstructions of variables such as SAT (Hakim et al., 2016; Steiger et al., 2014).

Here we use paleoclimate records from the LMR database version 1.0.0 (Anderson et al., 2019), which consists of subannually (averaged to annual resolution) and annually resolved paleoclimate data from the PAGES2k Phase 2 database (Emile-Geay et al., 2017), supplemented with Breitenmoser tree ring data (Breitenmoser et al., 2014) and proxy data from the National Centers for Environmental Information. The

number of available proxy records decreases before the twentieth century (e.g., Anderson et al., 2019; Tardif et al., 2019). Here we focus our analyses on the time period 1500–1850 CE to maximize proxy data availability; there are 548 proxies available in 1500 CE, 736 proxies in 1600 CE, and 2,354 proxies in 1850 CE.

We employ the regression-based proxy system modeling (PSM) approach (as opposed to a process-based PSM) described by Tardif et al. (2019) to map the climate model fields (e.g., SAT and precipitation) to the proxy measurements (e.g., tree ring width). We fit each paleoclimate record to the National Aeronautics and Space Administration Goddard Institute of Space Studies surface temperature version 4 data (GISTEMP; Hansen et al., 2010) over the 1880–2016 CE time period. To account for the impact of growing season on trees, we employ objectively determined seasonal predictors for each tree ring record (e.g., Tardif et al., 2019) fit to monthly GISTEMP and Global Precipitation and Climatology Centre version 6 data (Schneider et al., 2014) over the 1901–2010 CE time period. For all other proxy records, we calculate regressions among each proxy and annual mean GISTEMP data.

In order to account for uncertainty in proxy error and model covariance estimates, we generate 11 Monte Carlo (MC) iterations for each prior; each MC iteration uses 100 randomly drawn ensemble members from the prior and 75% of the proxy records. These "random" draws are seeded so that the same 100 calendar years are drawn from each of the 10 model priors, and the same 25% of proxies are withheld from each MC realization for each CMIP5 model. All analyses discussed here use LMR reconstructions of SAT composed of the 11 MC assimilation realizations. In all figures, we show results from averaging over the 1,100 ensemble member mean (100 ensemble members and 11 MC iterations for each CMIP5 prior). Results from this "grand ensemble mean" show the best verification against instrumental data (e.g., Hakim et al., 2016; Tardif et al., 2019). Local and regional covariances are quite similar across models, but spatially remote covariances can vary substantially (Figure S1 in the supporting information). To minimize the effects of proxy data influencing remote locations over unreasonably large distances, we localize the covariance estimate using the window function described in Gaspari and Cohn (1999) with a length scale of 25,000 km (distance to zero covariance). Further details about the LMR, including validation, sensitivity to model prior, PSM type, localization, and calibration method, can be found in Tardif et al. (2019), Steiger et al. (2014), Hakim et al. (2016), and Singh et al. (2018).

2.3. Calculating ROSI

Many climate indices rely on averages across large geographical regions; these regional averages may obscure relationships with the global mean if locations within a given geographic region, such as the North Pacific or Southern Ocean, do not vary coherently. Consequently, we test grid point relationships with GMSAT. Following Brown et al. (2015), we define a grid point as being a ROSI on interdecadal GMSAT if (1) local SAT shows a statistically significant relationship with GMSAT at a time lag of zero. To determine if local and GMSAT show a statistically significant relationship, from each grid point we draw 350 years of data (1500–1849 CE), randomize the order of the time series, smooth the time series, calculate the correlation against smoothed GMSAT, and repeat this procedure 1,000 times. This approach shows that local-global correlation must be greater than 0.3 to exceed the 95% confidence bound from the random draw. (2) The linear, zero-lag regression among local SAT and GMSAT is at least one. (3) Maximum cross correlations among local SAT and GMSAT show maximum correlations when local SAT leads GMSAT by at least one year, with a lead window up to 10 years in cross-correlation calculations. Grid points meeting these three criteria are stippled in Figures 2 and 4. A discussion of the potential limitations of this method can be found in section 3.

We limit our ROSI analysis of LMR and CMIP5 LM data to 1500–1850 CE. During this time period, there should be minimal impact of industrial era warming, and there is also relatively widespread proxy coverage for use in the LMR. We remove the linear trend from all grid points during this time period and account for latitude-dependent grid box size in all global averages. The relationships among local grid points and GMSAT in the CMIP5 LM data are relatively insensitive to the time period of analysis (e.g., 1500–1850 CE or 850–1850 CE; not shown).

Brown et al. (2015) use monthly data, but here we use CMIP5 annual mean SAT data to facilitate comparison with the annually resolved LMR data; when we compare CMIP5 monthly and annual mean results, similar regions show significant relationships with interdecadal GMSAT. Interdecadal ROSI are insensitive to cross-

correlation lead window (e.g., 5, 10, and 20 years). Here we use a third-order, 10-year low-pass, Butterworth filter (Butterworth, 1930) to smooth all SAT data before calculating relationships on interdecadal timescales among local grid points and GMSAT. We find that our results are insensitive to low-pass filter method (e.g., Butterworth versus Locally Weighted Scatterplot Smoothing) and low-pass filter cutoff (e.g., 10, 15, or 20-year cutoff; not shown).

2.4. Calculating Coherence of Global Mean and Local Temperature Variability

Although the regression-based ROSI method has been previously used to study regions driving GMSAT variability, this method uses GMSAT as the predictor in the regression calculations. Therefore, we compare results derived from the Brown et al. (2015) method with a multitaper spectral coherence approach (Mann & Park, 1993; Thomson, 1982). We use the coherence and phase of local SAT time series and GMSAT in time-frequency space to test where local variability shows a significant lead-lag relationship with global variability in CMIP5 and LMR data. At a given frequency (f), coherency estimates ($C(f)$) range between 0 and 1 with increasing values when the local and global time series covary at a given frequency. We also use the phase between the local and global mean variability to test the lead-lag relationship between these time series. A positive phase relationship indicates that local variability leads global variability, whereas a negative phase would suggest that local variability lags global variability at this frequency. Regions in coherency maps are stippled where two criteria are met: (1) local versus global coherency exceeds a noise threshold at the 95% confidence level. To generate the 95% upper confidence bound for the interdecadal coherence calculations, from each grid point we draw 350 years of data (1500–1849 CE), randomize the order of the time series, calculate the mean coherence with GMSAT at interdecadal timescales, and repeat this procedure 1,000 times; this method shows that mean interdecadal coherence must exceed 0.44 to surpass the 95% noise threshold (e.g., Amos & Koopmans, 1963; Priestley, 1981). We choose this 350-year time series length to correspond with the length of the 1500–1849 CE time period from the coherence analyses conducted on the CMIP5 LM and LMR data, but a slightly longer or shorter time series length (e.g., 500 years of data from 1350 to 1849 CE) does not significantly change the coherence noise threshold. (2) The phase relationship between local and global mean temperatures is positive, implying that local variability leads global mean variability. Although coherence is calculated at multiple frequency ranges, here we use the average coherency and phase at interdecadal ($f < 0.1$) timescales to correspond with the interdecadal ROSI calculations in section 2.3.

3. Results

Traditionally, instrumental, paleoclimate, and climate model data have been used to study internal and externally forced climate variability (e.g., Delworth et al., 1993; Jones, 1989; Manabe & Stouffer, 1996; Mann et al., 1995; Mann & Park, 1994; Stouffer et al., 1994). Instrumental, climate model, and paleoclimate data indicate that physically driven, coupled modes of internal variability may play a role in some degree of regional and global temperature variations (e.g., Kushnir, 1994; Mann & Park, 1993, 1994; Mann et al., 1995; Manabe & Stouffer, 1996). However, each of these data sources has its own spatial and temporal limitations, and climate models often disagree on the regions that influence GMSAT (e.g., Brown et al., 2015). Here we contrast results from 10 CMIP5 LM simulations and the LMR. We focus on ocean regions that may lead GMSAT variability due to the potential role of the ocean in driving low-frequency climate variability (e.g., Bjerknes, 1964; Delworth et al., 1993; Drijfhout, 2018; Frankignoul & Hasselmann, 1977; Hasselmann, 1976; Xie et al., 2016).

Figure 1 shows time series of interdecadal GMSAT in the 10 CMIP5 LM and LMR iterations using these CMIP5 simulations as priors. The magnitude of GMSAT variability is lower in the LMR than in the CMIP5 LM data. The lower magnitude of variability in the LMR is due to a combination of factors, including the use of a fixed prior for each year, disagreement in proxy time series, imperfect proxy PSMs, and sparse proxy coverage (e.g., Singh et al., 2018). The use of a fixed prior means that in the absence of proxy information, the ensemble mean anomaly of the reconstruction collapses to zero. Therefore, in years with geographically sparse and/or noisy proxy data, the ensemble mean global mean time series shows lower magnitude variability than the variability in the model priors.

Temperature anomalies following large volcanic eruptions (e.g., 1601, 1641, 1695, 1808, 1815 CE; Gao et al., 2008; Sigl et al., 2015) show global cooling in both CMIP5 LM and the LMR (Figure 1), but the proxy-based
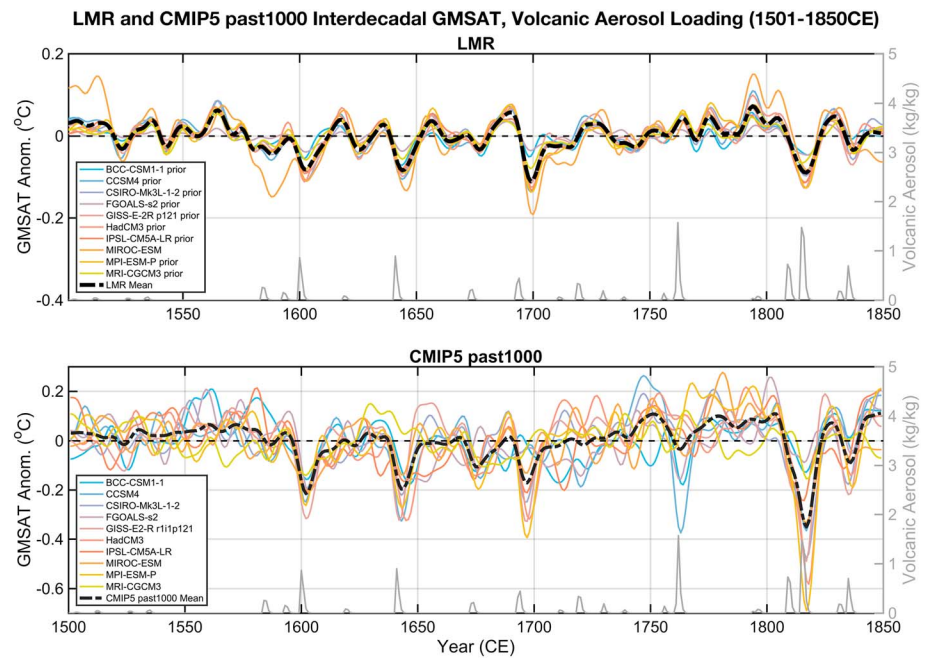
Figure 1. Time series of global mean surface air temperature (GMSAT) at interdecadal (>10 years) timescales in 10 LMR iterations (top), each of which uses a CMIP5 Last Millennium simulation (bottom) as a model prior. Linear trends have been removed, and time series are smoothed with a 10-year low-pass filter (section 2). Anomalies are relative to the 1500–1850 CE mean. Note the different y axis scales in the top and bottom panels. Gray lines show the volcanic aerosol mass loading time series used in the NCAR CCSM4 past1000 experiment (Gao et al., 2008; Landrum et al., 2013). LMR = Last Millennium Reanalysis; CMIP5 = Coupled Model Intercomparison Project, Phase 5.

reconstructions suggest less cooling following these eruptions relative to internal variability (e.g., Atwood et al., 2016). Although the relative magnitude of GMSAT variability in the LMR is lower than the magnitude of variability in the CMIP5 data, the relationships between local and global variability show similar magnitudes and patterns in these two data sources (e.g., Figures 2–5).

We compare results from all CMIP5 LM simulations and LMR reconstructions to (1) compare CMIP5 LM models and LMR regions that significantly influence interdecadal GMSAT, (2) test if LMR results are sensitive to CMIP5 model prior, and (3) provide a comparison of each CMIP5 model prior with its associated LMR output. This comparison allows us to better identify sensitivity in the LMR to model prior covariances.

3.1. CMIP5 LM Surface Temperature

Here we compare ROSI results for CMIP5 LM models for the recent preinstrumental era. CMIP5 preindustrial control (Brown et al., 2015) and LM simulations show that the tropical Pacific influences GMSAT on interannual timescales (not shown). There is also general agreement in the instrumental record that the tropical Pacific plays a significant role in influencing GMSAT on these timescales (e.g., Halpert & Ropelewski, 1992; Mann & Park, 1994; Zhang et al., 1997).

CMIP5 LM models disagree on which regions are associated with GMSAT on interdecadal timescales. Although transient forcing in CMIP5 LM simulations appears to synchronize temperature variability over the lower latitudes (Figure 2) as compared to CMIP5 preindustrial control simulations (Figures S2 and S3), there is still little intermodel agreement in the CMIP5 LM simulations in terms of which regions show significant lead-lag relationships with GMSAT. For example, certain CMIP5 LM models such as MIROC-ESM and MPI-ESM-P suggest that the tropical Pacific influences interdecadal GMSAT variability. However, the remaining CMIP5 LM models show that varying combinations of the Southern Ocean, North Pacific, or North Atlantic may significantly influence interdecadal GMSAT (Figure 2). Although these models may broadly agree on which ocean basins are associated with GMSAT, there are large intermodel
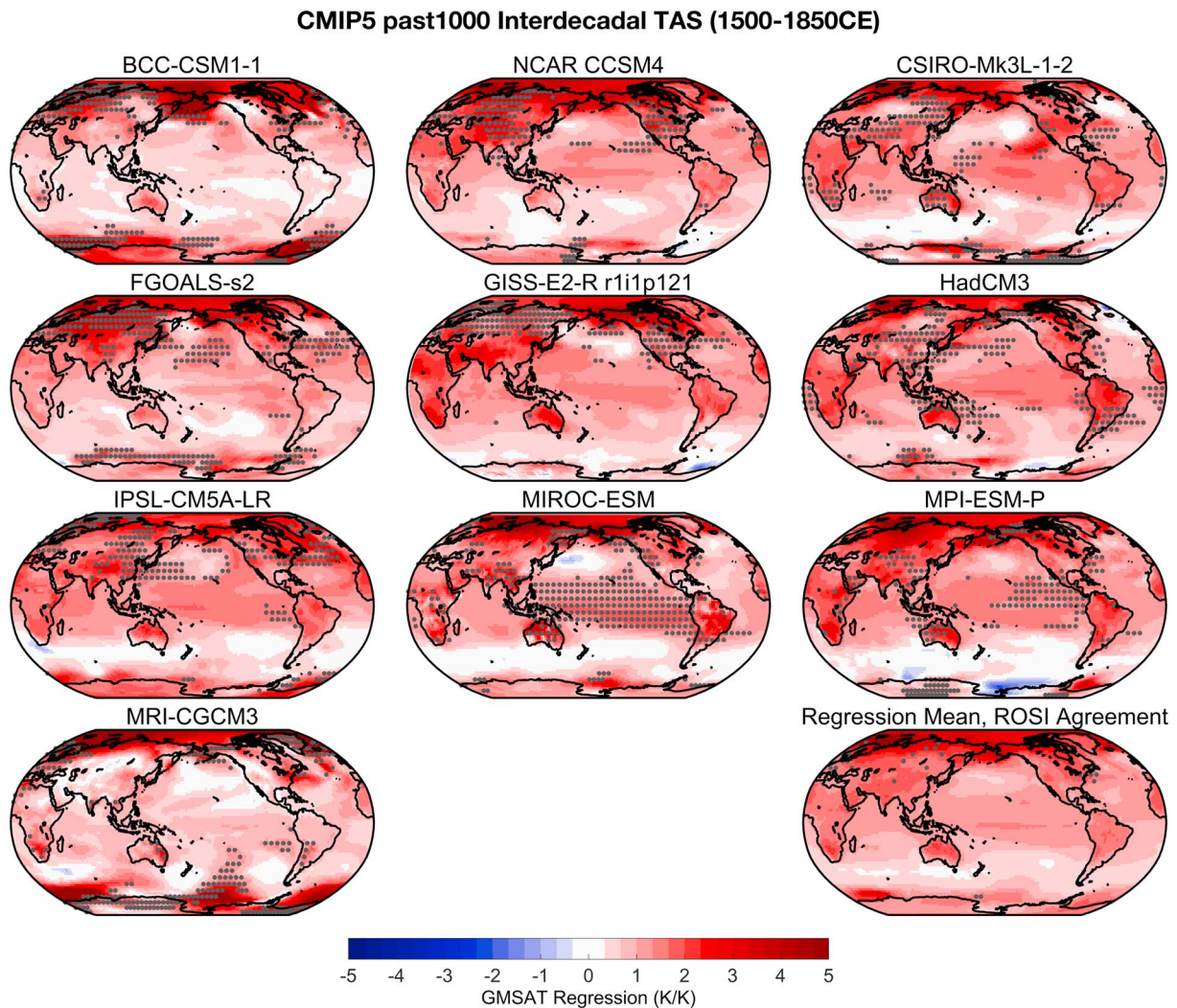
Figure 2. Regressions of global mean surface air temperature (GMSAT) on local temperature at interdecadal (>10 years) timescales in the CMIP5 Last Millennium (past1000) simulations, 1500–1850 CE. Stippling denotes local geographic regions of significant influence (ROSI) on GMSAT at interdecadal timescales (section 2). Map in lower right corner shows mean regressions across all CMIP5 Last Millennium models, with stippling showing grid points where at least 6 out of 10 models agree a location is a ROSI. CMIP5 = Coupled Model Intercomparison Project, Phase 5.

disagreements on specific local regions within these basins (e.g., Brown et al., 2015). For example, models such as BCC-CSM1-1, FGOALS-s2, HadCM3, and IPSL-CM5A-LR suggest that various parts of the northwest Pacific are important, whereas CCSM4, GISS-E-2R, and MPI-ESM-P suggest the northeastern extratropical Pacific (Figure 2). A few models agree on specific ROSI regions, but there are effectively no regions where at least 6 out of 10 of the CMIP5 LM models agree that a region influences interdecadal GMSAT. The one exception is a small geographic region in the extratropical North Atlantic off the coast of eastern North America (lower right panel, Figure 2), where most models show some influence on interdecadal GMSAT.

The regression-based ROSI approach shows which regions are most strongly associated with GMSAT variability, but this method uses GMSAT as the predictor in the regression calculations (Brown et al., 2015). Therefore, we test these regression-based results using a spectral coherence approach (section 2). The shading in Figure 3 shows the mean interdecadal (>10-year period) coherence between local temperature and GMSAT variability. Stippling shows where coherence is significant, and local temperature leads GMSAT at interdecadal timescales (section 2). Although the shading in these interdecadal coherency maps generally shows a strong relationship between the tropics and GMSAT, there is little agreement among models in terms of which local regions both lead and show a significant relationship with GMSAT at these
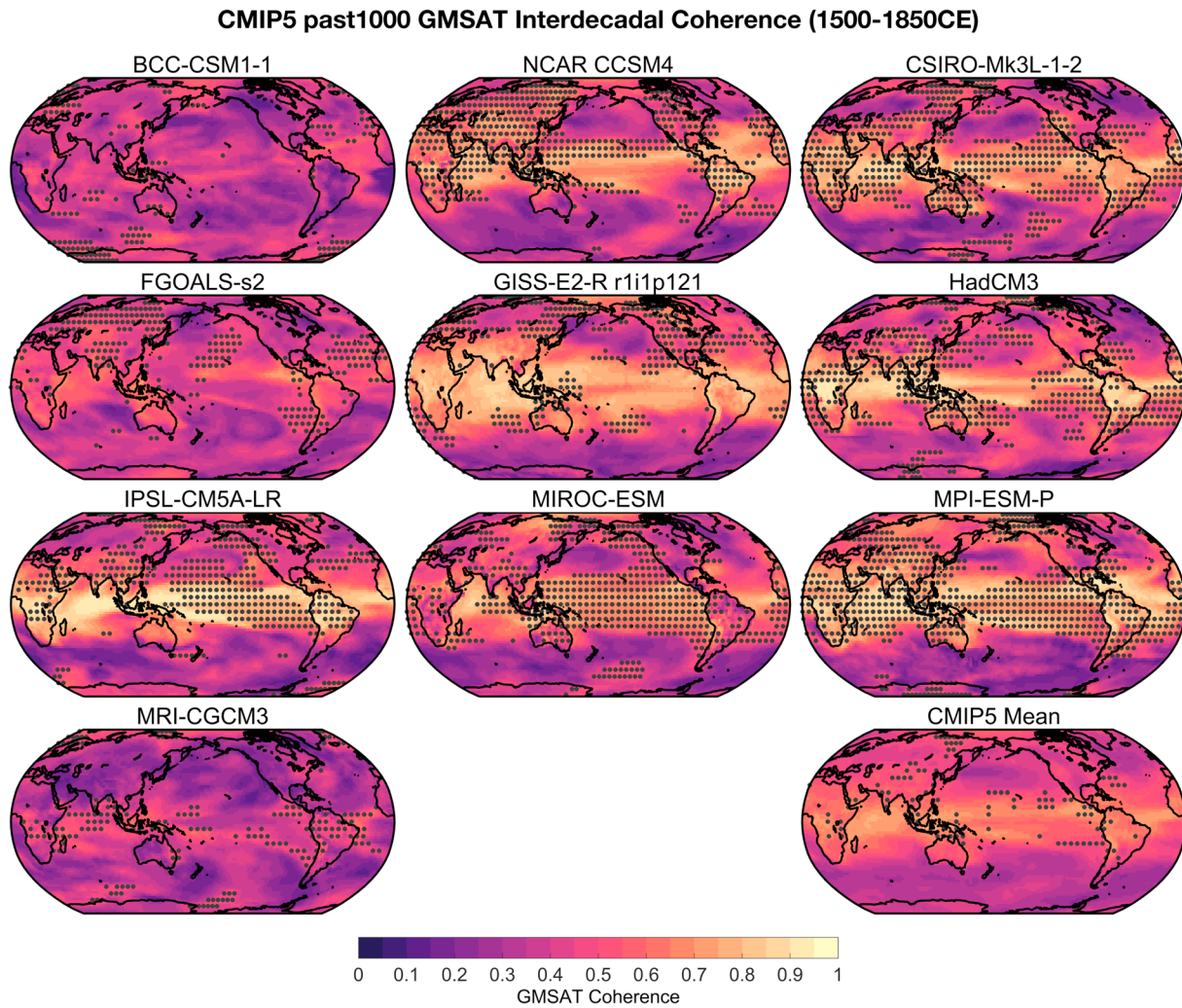
Figure 3. Spectral coherence ($C(f)$) of local temperature and global mean surface air temperature (GMSAT) at interdecadal ($f < 0.1$) timescales in the CMIP5 Last Millennium (past1000) simulations, 1500–1850 CE. Stippling denotes local geographic regions where the global versus local relationship exceeds the noise threshold, and local variability leads global variability at interdecadal timescales (section 2). Map in lower right corner shows mean coherence across all CMIP5 Last Millennium models, with stippling showing grid points where at least 6 out of 10 models agree that a location shows a significant lead relationship with the global mean at interdecadal timescales. CMIP5 = Coupled Model Intercomparison Project, Phase 5.

timescales (Figure 3). These spectral coherency-based results generally confirm the major results of the regression ROSI-based method: there is little agreement among CMIP5 LM simulations in terms of which local regions lead GMSAT and show significant relationships with GMSAT at interdecadal timescales.

3.2. LMR Surface Temperature

We have generated output from 10 LMR experiments (section 2), one for each of the 10 CMIP5 LM models as prior for the data assimilation algorithm. We compare LMR results using these different model priors to test if our results are robust to the model prior. In Figure 4, we show regressions among GMSAT and local SAT in each LMR experiment, with stippling showing ROSI on interdecadal GMSAT. Results emphasize primarily extratropical locations as the key regions that influence interdecadal GMSAT variability, but five of the LMR experiments (using BCC-CSM1-1, CCSM4, FGOALS-s2, HadCM3, IPSL-CM5A-LR, and MRI-CGCM3 as model priors) also show that varying parts of the central and eastern tropical Pacific are ROSI. The stippling in the lower right panel in Figure 4 shows where at least 6 out of 10 LMR experiments agree that a region significantly influences GMSAT. Almost all LMR configurations that we tested show central Asia, the extratropical northeastern North Pacific region near the Gulf of Alaska, and the North Atlantic region near Greenland and Iceland are ROSI.
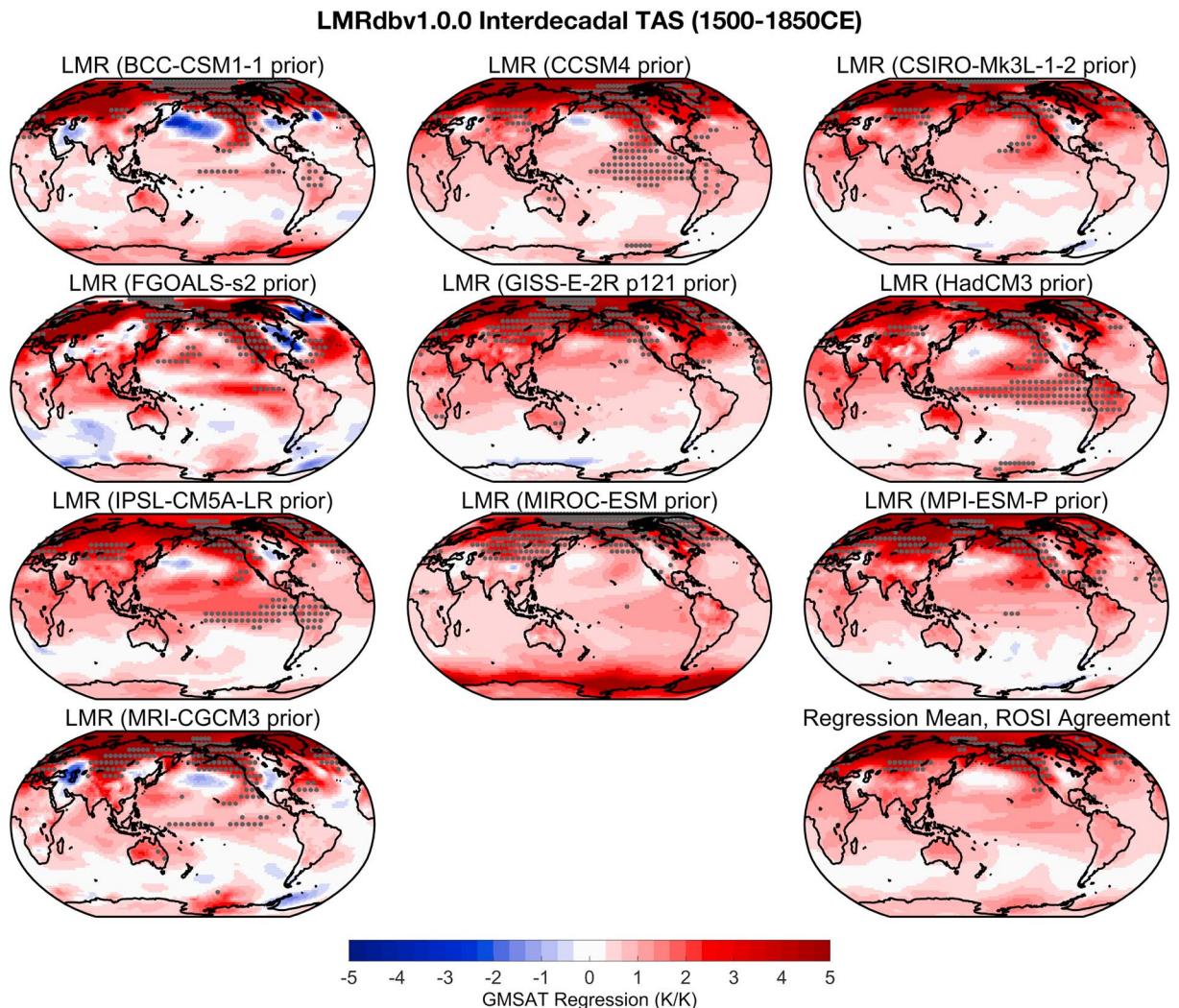
Figure 4. Regressions of global mean surface air temperature (GMSAT) on local temperature at interdecadal (>10 years) timescales in 10 iterations of the LMR, each using one of the Coupled Model Intercomparison Project, Phase 5 Last Millennium simulations (section 2) as the model prior, 1500–1850 CE. Stippling denotes local geographic regions of significant influence (ROSI) on GMSAT at interdecadal timescales (section 2). Map in lower right corner shows mean regressions across all LMR iterations, with stippling marking regions in which at least 6 out of 10 LMR experiments agree that a location is a ROSI. LMR = Last Millennium Reanalysis.

These results are relatively insensitive to the number of proxies used. For example, we conducted separate LMR experiments in which we withheld 0%, 25%, 50%, or 75% of proxies in each MC iteration of the reconstruction. We also conducted an LMR experiment in which we limited the proxy network to the ~500 annually resolved paleoclimate PAGES2k Phase 2 records (Emile-Geay et al., 2017). Moreover, we tested a fixed proxy network using only proxies with constant coverage through the time period of analysis. All of these experiments show similar results (Figure S4). Furthermore, these regions tend to show significant relationships with the GMSAT in each separate LMR MC iteration (as opposed to the 11 MC iteration mean, which is shown in Figure 4). The consistency of these results suggests that the influence of extratropical regions in the North Pacific and North Atlantic on interdecadal GMSAT variability is a robust signal in the preindustrial climate system as reconstructed by current annually resolved proxy data in the LMR framework.

As we did for the CMIP5 LM simulations, here we compare the LMR regression-based ROSI results to those results from the spectral coherence method. The shading in Figure 5 shows the mean interdecadal (>10-year period) coherence between local temperature and GMSAT variability in the LMR, and stippling shows where this coherency is significant and local temperature leads GMSAT at interdecadal
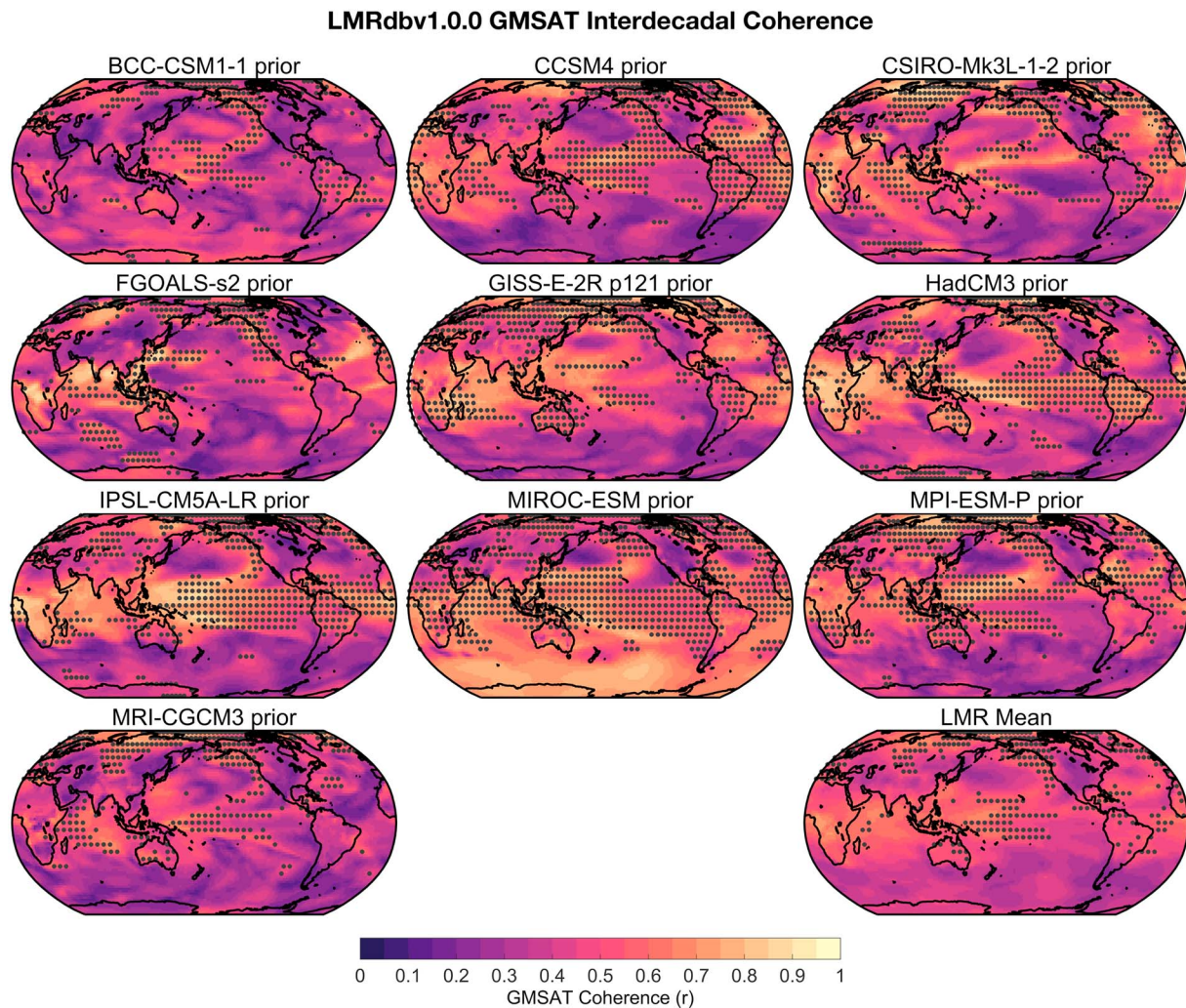
Figure 5. Spectral coherence ($C(f)$) of local temperature and global mean surface air temperature (GMSAT) at interdecadal ($f < 0.1$) timescales in 10 iterations of the LMR, each using one of the Coupled Model Intercomparison Project, Phase 5 Last Millennium simulations (section 2) as the model prior 1500–1850 CE. Stippling denotes local geographic regions where the global versus local relationship exceeds the noise threshold, and local variability leads global variability at interdecadal timescales (section 2). Map in lower right corner shows mean coherence across all LMR iterations, with stippling showing grid points where at least 6 out of 10 LMR experiments agree that a location shows a significant lead relationship with the global mean at interdecadal timescales. LMR = Last Millennium Reanalysis.

timescales (section 2). Although approximately half of the LMR coherency maps show a strong relationship between the tropics and GMSAT at interdecadal timescales, the regions that lead GMSAT are similar to those found in the ROSI approach: north central Asia, the North Pacific, North Atlantic, Arctic, and central Pacific (Figure 5). The stippling in these coherency maps generally confirms the regression-based ROSI LMR results that the North Pacific, North Atlantic, and central Asia regions have a significant leading relationship with GMSAT at interdecadal timescales.

4. Discussion and Conclusions

Despite the potential importance of low-frequency climate variability, we have a limited understanding of the drivers of GMSAT variability at interdecadal timescales. Here we use the LMR framework to examine the geographic regions where local variability shows a significant relationship with interdecadal GMSAT variability. The LMR uses an ensemble Kalman filter data assimilation approach to combine paleoclimate data and climate model simulations to generate annually resolved multivariate field reconstructions of the instrumental and preinstrumental era (e.g., Hakim et al., 2016; Steiger et al., 2014; Tardif et al., 2019).

We test if CMIP5 LM simulations agree on which regions influence GMSAT at interdecadal timescales and contrast these model-based results with results from the LMR. A coherence analysis of local SAT and GMSAT indicates that there is some agreement among CMIP5 LM simulations that the tropics may influence interdecadal GMSAT variability (Figure 3). Although individual CMIP5 simulations show general agreement on ocean basins driving GMSAT, there is little agreement on which local regions drive GMSAT at interdecadal timescales (Figures 2 and 3). By contrast, the LMR consistently shows that the middle- to high-latitude North Pacific, high-latitude North Atlantic, and central Asia tend to significantly influence interdecadal GMSAT variability (Figures 4 and 5). Despite differences between the CMIP LM simulations and LMR, the ensemble means of the CMIP5 LM and LMR regression and coherence maps reveal general agreement in terms of which regions are related to interdecadal GMSAT (bottom right corners Figures 2 and 4). Both data sources agree that GMSAT is strongly related to tropical and high-latitude variability over oceans, but the midlatitude Southern Ocean and central, midlatitude North Pacific show weaker relationships with GMSAT, especially when relying on the regression-based ROSI method. Indeed, recent model-based work has shown that prescribed heat fluxes in the North Pacific may play an important role in driving global climate variability (Praetorius et al., 2018), and the North Atlantic can influence low-frequency GMSAT variability (Stolpe et al., 2018).

Although the LMR-based results appear to be robust, there are several limitations associated with using the LMR framework to combine the available paleoclimate network and climate model data to examine local SAT variability. We discuss potential limitations related to (1) paleoclimate data locations and (2) model covariances in the following two paragraphs. We then include a brief discussion of pseudoproxy experimental results that test the ability of the LMR framework to reconstruct decadal variability using model covariances combined with the LMR database proxy locations.

1. Potential limitations related to paleoclimate data locations: Most of the annually resolved paleoclimate data used in the reconstructions presented here are from trees in the Northern Hemisphere; this uneven, Northern Hemisphere-weighted proxy network may bias our view of preinstrumental climate variability. Yet the air temperature results presented here appear robust across a variety of LMR experimental configurations withholding various percentages of proxies (Figure S4) and if we use the Mann et al. (2009) Climate Field Reconstruction SAT data (Figure S5). However, the northeastern Pacific ROSI in the LMR does not appear when we withhold all North American tree ring records from our LMR reconstruction. This decreased signal in the Northern Hemisphere is perhaps not surprising given the number of proxy records (and relative proportion of information) from North American trees. More paleoclimate data are needed to provide information about Southern Hemisphere, middle- to high-latitude climate variability, and its potential drivers. A temporally and geographically expanded, annually resolved, paleoclimate network in the tropics and over the Southern Hemisphere would likely improve regional temperature reconstructions.

2. Potential limitations related to covariances in the climate model priors: If a prior consistently misrepresents climate variability, the LMR results will likely also reflect this model bias. For example, if an internal mode of variability (e.g., the El Niño–Southern Oscillation) unrealistically dominates a model's covariance, then the spatial teleconnections associated with this mode of variability could influence the LMR posterior. Here we attempt to circumvent this potential limitation by creating multiple LMR reconstructions using various climate model priors and report results where most LMR reconstructions agree.

To test the ability of the LMR framework to reconstruct the timing of decadal temperature variability over data-sparse regions, we conduct a series of pseudoproxy experiments. In these pseudoproxy experiments, we sample SAT pseudo-observations of 2-m air temperature from the model data at the LMR database proxy locations. We then add noise to each pseudo-observation to match the signal-to-noise ratio of its associated proxy record. We use these pseudo-observations in the data assimilation framework to reconstruct SAT 1500–1849 CE (see Text S1 for a more detailed description of the pseudoproxy experimental setup). Grid point correlations between interdecadal SAT in the model and the pseudoproxy posteriors (1500–1849 CE) show that the proxy locations used in the LMR framework over this time period capture the timing of decadal variability over most ocean regions, with the exception of certain regions in the Southern Ocean (Figure S6), where variability is underestimated by the LMR.

Despite the limitations of the data assimilation framework, the LMR provides a new data-model hybrid perspective on preinstrumental climate variability using the latest annually resolved paleoclimate data. These field reconstructions of past climate can be used to better constrain the dynamics of past climate variability. Specifically, the LMR results presented here show that the central and northern Pacific, North Atlantic, and central Asia regions are associated with interdecadal air temperature variability, which are not as consistently evident in CMIP5 simulations of the LM. We hypothesize that in CMIP5 LM simulations, "top-down" external forcing (e.g., cooling following volcanic eruptions) appears to drive much of the low-frequency climate variability, particularly in the tropics (e.g., Parsons et al., 2017). By contrast, the LMR could be capturing a stronger "bottom up" signal of internal, low-frequency variability from within the climate system. Although we have not examined the physical mechanisms that may drive preindustrial, internal climate variability, a possible source of bottom up natural decadal variability could include heat fluxes from middle-latitude and high-latitude ocean regions, such as the North Atlantic or North Pacific (e.g., Praetorius et al., 2018; Stolpe et al., 2018) or the Southern Ocean. These ocean-atmosphere coupled relationships could be further investigated by examining surface energy budgets and ocean heat content in the LMR and model priors to examine the mechanisms responsible for driving climate variability. Furthermore, here we examine grid point relationships with GMSAT, but spatially consistent climate modes associated with low-frequency climate variability could be examined in both model simulations and the LMR (e.g., Wills et al., 2019, 2018). Among other advances, the LMR paleoclimate data assimilation framework could be improved by employing physically based proxy system forward models (e.g., Dee et al., 2015, 2016, 2017), and linear inverse modeling methods could increase year-to-year memory in LMR reconstructions (e.g., Perkins & Hakim, 2017). Further studies of mismatches (and agreements) in the regional patterns and timing of variability in the LMR and climate model data may provide some insights into the robustness of model results (e.g., PAGES 2k Consortium, 2019) or how to improve model simulations of the preindustrial climate.

References

Anderson, D., Tardif, R., Horlick, K., Erb, M., Hakim, G., Noone, D., et al. (2019). Additions to the Last Millennium Reanalysis multi-proxy database. *Data Science Journal*, *18*(1). https://doi.org/10.5334/dsj-2019-002

Amos, D. E. & Koopmans, L. H. (1963). *Tables of the distribution of the coefficient of coherence for stationary bivariate Gaussian processes*.

Atwood, A., Wu, E., Frierson, D., Battisti, D., & Sachs, J. (2016). Quantifying climate forcings and feedbacks over the last millennium in the CMIP5–PMIP3 models. *Journal of Climate*, *29*(3), 1161–1178. https://doi.org/10.1175/JCLI-D-15-0063.1

Bjerknes, J. (1964). Atlantic air-sea interaction. *Advances in Geophysics*, *10*, 1–82. https://doi.org/10.1016/S0065-2687(08)60005-9

Breitenmoser, P. D., Brönnimann, S., & Frank, D. (2014). Forward modelling of tree-ring width and comparison with a global network of tree-ring chronologies. *Climate of the Past*, *10*(2), 437–449. https://doi.org/10.5194/cp-10-437-2014

Brown, P. T., Li, W., Jiang, J. H., & Su, H. (2016). Spread in the magnitude of climate model interdecadal global temperature variability traced to disagreements over high-latitude oceans. *Geophysical Research Letters*, *43*, 12,543–12,549. https://doi.org/10.1002/2016GL071442

Brown, P. T., Li, W., & Xie, S. (2015). Regions of significant influence on unforced global mean surface air temperature variability in climate models. *Journal of Geophysical Research: Atmospheres*, *120*, 480–494. https://doi.org/10.1002/2014JD022576

Brown, P. T., Ming, Y., Li, W., & Hill, S. A. (2017). Change in the magnitude and mechanisms of global temperature variability with warming. *Nature Climate Change*, *7*(10), 743–748. https://doi.org/10.1038/nclimate3381

Butterworth, S. (1930). On the theory of filter amplifiers. *Wireless Engineer*, *7*, 536–541.

Compo, G. P., Whitaker, J. S., Sardeshmukh, P. D., Matsui, N., Allan, R. J., Yin, X., et al. (2011). The twentieth century reanalysis project. *Quarterly Journal of the Royal Meteorological Society*, *137*(654), 1–28. https://doi.org/10.1002/qj.776

Crowley, T. J. (2000). Causes of climate change over the past 1000 years. *Science*, *289*(5477), 270–277. https://doi.org/10.1126/science.289.5477.270

Dee, S., Emile-Geay, J., Evans, M. N., Allam, A., Steig, E. J., & Thompson, D. M. (2015). PRYSM: An open-source framework for PRoxY System Modeling, with applications to oxygen-isotope systems. *Journal of Advances in Modeling Earth Systems*, *7*, 1220–1247. https://doi.org/10.1002/2015MS000447

Dee, S., Parsons, L., Loope, G., Overpeck, J., Ault, T., & Emile-Geay, J. (2017). Improved spectral comparisons of paleoclimate models and observations via proxy system modeling: Implications for multi-decadal variability. *Earth and Planetary Science Letters*, *476*, 34–46. https://doi.org/10.1016/j.epsl.2017.07.036

Dee, S. G., Steiger, N. J., Emile-Geay, J., & Hakim, G. J. (2016). On the utility of proxy system models for estimating climate states over the common era. *Journal of Advances in Modeling Earth Systems*, *8*, 1164–1179. https://doi.org/10.1002/2016MS000677

Delworth, T., Manabe, S., & Stouffer, R. (1993). Interdecadal variations of the thermohaline circulation in a coupled ocean-atmosphere model. *Journal of Climate*, *6*(11), 1993–2011. https://doi.org/10.1175/1520-0442(1993)006<1993:IVOTTC>2.0.CO;2

Drijfhout, S. (2018). The relation between natural variations in ocean heat uptake and global mean surface temperature anomalies in CMIP5. *Scientific Reports*, *8*(1), 7402. https://doi.org/10.1038/s41598-018-25342-7

Emile-Geay, J., McKay, N. P., Kaufman, D. S., von Gunten, L., Wang, J., Anchukaitis, K. J., et al. (2017). A global multiproxy database for temperature reconstructions of the Common Era. *Scientific Data*, *4*.

Frankignoul, C., & Hasselmann, K. (1977). Stochastic climate models.2. Application to sea-surface temperature anomalies and thermocline variability. *Tellus*, *29*, 289–305.

Gao, C., Robock, A., & Ammann, C. (2008). Volcanic forcing of climate over the past 1500 years: An improved ice core-based index for climate models. *Journal of Geophysical Research*, *113*, D23111. https://doi.org/10.1029/2008JD010239

Gaspari, G., & Cohn, S. E. (1999). Construction of correlation functions in two and three dimensions. *Quarterly Journal of the Royal Meteorological Society*, *125*(554), 723–757. https://doi.org/10.1002/qj.49712555417

Goosse, H., Renssen, H., Timmermann, A., & Bradley, R. S. (2005). Internal and forced climate variability during the last millennium: A model-data comparison using ensemble simulations. *Quaternary Science Reviews*, *24*(12-13), 1345–1360. https://doi.org/10.1016/j.quascirev.2004.12.009

Hakim, G. J., Emile-Geay, J., Steig, E. J., Noone, D., Anderson, D. M., Tardif, R., et al. (2016). The last millennium climate reanalysis project: Framework and first results. *Journal of Geophysical Research: Atmospheres*, *121*, 6745–6764. https://doi.org/10.1002/2016JD024751

Halpert, M. S., & Ropelewski, C. F. (1992). Surface temperature patterns associated with the Southern Oscillation. *Journal of Climate*, *5*(6), 577–593. https://doi.org/10.1175/1520-0442(1992)005<0577:STPAWT>2.0.CO;2

Hansen, J., Ruedy, R., Sato, M., & Lo, K. (2010). Global surface temperature change. *Reviews of Geophysics*, *48*, RG4004. https://doi.org/10.1029/2010RG000345

Hasselmann, K. (1976). Stochastic climate models.1. Theory. *Tellus*, *28*, 473–485.

Hawkins, E., & Sutton, R. (2009). The potential to narrow uncertainty in regional climate predictions. *Bulletin of the American Meteorological Society*, *90*(8), 1095–1108. https://doi.org/10.1175/2009BAMS2607.1

Hegerl, G. C., Brönnimann, S., Schurer, A., & Cowan, T. (2018). The early 20th century warming: Anomalies, causes, and consequences. *Wiley Interdisciplinary Reviews: Climate Change*, *9*, e522.

Jones, P. (1989). The influence of ENSO on global temperatures. *Climate Monitor*, *17*, 80–89.

Kirtman, B., S. Power, A. Adedoyin, G. Boer, R. Bojariu, I. Camilloni, et al. (2013), Near-term climate change: Projections and predictability.

Knutson, T. R., Zhang, R., & Horowitz, L. W. (2016). Prospects for a prolonged slowdown in global warming in the early 21st century. *Nature Communications*, *7*(1), 13,676. https://doi.org/10.1038/ncomms13676

Kushnir, Y. (1994). Interdecadal variations in North Atlantic sea surface temperature and associated atmospheric conditions. *Journal of Climate*, *7*, 141–157.

Landrum, L., Otto-Bliesner, B. L., Wahl, E. R., Conley, A., Lawrence, P. J., Rosenbloom, N., & Teng, H. (2013). Last millennium climate and its variability in CCSM4. *Journal of Climate*, *26*(4), 1085–1111. https://doi.org/10.1175/JCLI-D-11-00326.1

Manabe, S., & Stouffer, R. (1996). Low-frequency variability of surface air temperature in a 1000-year integration of a coupled atmosphere-ocean-land surface model. *Journal of Climate*, *9*(2), 376–393. https://doi.org/10.1175/1520-0442(1996)009<0376:LFVOSA>2.0.CO;2

Mann, M. E., & Park, J. (1993). Spatial correlations of interdecadal variation in global surface temperatures. *Geophysical Research Letters*, *20*(11), 1055–1058. https://doi.org/10.1029/93GL00752

Mann, M. E., & Park, J. (1994). Global-scale modes of surface temperature variability on interannual to century timescales. *Journal of Geophysical Research*, *99*(D12), 25,819–25,833. https://doi.org/10.1029/94JD02396

Mann, M. E., Park, J., & Bradley, R. (1995). Global interdecadal and century-scale climate oscillations during the past five centuries. *Nature*, *378*(6554), 266–270. https://doi.org/10.1038/378266a0

Mann, M. E., Zhang, Z., Rutherford, S., Bradley, R. S., Hughes, M. K., Shindell, D., et al. (2009). Global signatures and dynamical origins of the little ice age and medieval climate anomaly. *Science*, *326*(5957), 1256–1260. https://doi.org/10.1126/science.1177303

Masson-Delmotte, V., Schulz, M., Abe-Ouchi, A., Beer, J., Ganopolski, A., Gonzalez Rouco, J. F., et al. (2013). Information from paleoclimate archives. In *Climate Change 2013: The Physical Science Basis* (pp. 383–464). Cambridge: Cambridge University Press.

Meehl, G. A., Arblaster, J. M., Fasullo, J. T., Hu, A., & Trenberth, K. E. (2011). Model-based evidence of deep-ocean heat uptake during surface-temperature hiatus periods. *Nature Climate Change*, *1*(7), 360–364. https://doi.org/10.1038/nclimate1229

Meehl, G. A., Hu, A., Arblaster, J. M., Fasullo, J., & Trenberth, K. E. (2013). Externally forced and internally generated decadal climate variability associated with the Interdecadal Pacific Oscillation. *Journal of Climate*, *26*, 7298–7310.

PAGES 2k Consortium (2019). Consistent multi-decadal variability in global temperature reconstructions and simulations over the Common Era. *Nature Geoscience*, *12*, 643–649.

Parsons, L. A., Loope, G. R., Overpeck, J. T., Ault, T. R., Stouffer, R., & Cole, J. E. (2017). Temperature and precipitation variance in CMIP5 simulations and paleoclimate records of the last millennium. *Journal of Climate*, *30*, 8885–8912.

Perkins, W. A., & Hakim, G. J. (2017). Reconstructing paleoclimate fields using online data assimilation with a linear inverse model. *Climate of the Past*, *13*(5), 421–436. https://doi.org/10.5194/cp-13-421-2017

Praetorius, S., Rugenstein, M., Persad, G., & Caldeira, K. (2018). Global and Arctic climate sensitivity enhanced by changes in North Pacific heat flux. *Nature Communications*, *9*(1), 3124. https://doi.org/10.1038/s41467-018-05337-8

Priestley, M. B. (1981). *Spectral analysis and time series*. London: Academic Press.

Rind, D., Goldberg, R., & Ruedy, R. (1989). Change in climate variability in the 21st century. *Climatic Change*, *14*(1), 5–37. https://doi.org/10.1007/BF00140173

Schmidt, G. A., Jungclaus, J., Ammann, C., Bard, E., Braconnot, P., Crowley, T., et al. (2011). Climate forcing reconstructions for use in PMIP simulations of the last millennium (v1. 0). *Geoscientific Model Development*, *4*(1), 33–45. https://doi.org/10.5194/gmd-4-33-2011

Schneider, U., Becker, A., Finger, P., Meyer-Christoffer, A., Ziese, M., & Rudolf, B. (2014). GPCC's new land surface precipitation climatology based on quality-controlled in situ data and its role in quantifying the global water cycle. *Theoretical and Applied Climatology*, *115*(1-2), 15–40. https://doi.org/10.1007/s00704-013-0860-x

Schurer, A. P., Hegerl, G. C., Mann, M. E., Tett, S. F., & Phipps, S. J. (2013). Separating forced from chaotic climate variability over the past millennium. *Journal of Climate*, *26*(18), 6954–6973. https://doi.org/10.1175/JCLI-D-12-00826.1

Schurer, A. P., Hegerl, G. C., & Obrochta, S. P. (2015). Determining the likelihood of pauses and surges in global warming. *Geophysical Research Letters*, *42*, 5974–5982. https://doi.org/10.1002/2015GL064458

Sigl, M., Winstrup, M., McConnell, J. R., Welten, K. C., Plunkett, G., Ludlow, F., et al. (2015). Timing and climate forcing of volcanic eruptions for the past 2,500 years. *Nature*, *523*(7562), 543–549. https://doi.org/10.1038/nature14565

Singh, H. K., Hakim, G. J., Tardif, R., Emile-Geay, J., & Noone, D. C. (2018). Insights into Atlantic multidecadal variability using the Last Millennium Reanalysis framework. *Climate of the Past*, *14*(2), 157–174. https://doi.org/10.5194/cp-14-157-2018

Steiger, N. J., Hakim, G. J., Steig, E. J., Battisti, D. S., & Roe, G. H. (2014). Assimilation of time-averaged pseudoproxies for climate reconstruction. *Journal of Climate*, *27*(1), 426–441. https://doi.org/10.1175/JCLI-D-12-00693.1

Steiger, N. J., Smerdon, J. E., Cook, E. R., & Cook, B. I. (2018). A reconstruction of global hydroclimate and dynamical variables over the Common Era. *Scientific Data*, *5*(1). https://doi.org/10.1038/sdata.2018.86

Steinman, B. A., Mann, M. E., & Miller, S. K. (2015). Climate change. Atlantic and Pacific multidecadal oscillations and Northern Hemisphere temperatures. *Science*, *347*(6225), 988–991. https://doi.org/10.1126/science.1257856

Stolpe, M. B., Medhaug, I., & Knutti, R. (2017). Contribution of Atlantic and Pacific multidecadal variability to twentieth-century temperature changes. *Journal of Climate*, *30*(16), 6279–6295. https://doi.org/10.1175/JCLI-D-16-0803.1

Stolpe, M. B., Medhaug, I., Sedlácek, J., & Knutti, R. (2018). Multidecadal variability in global surface temperatures related to the Atlantic Meridional Overturning Circulation. *Journal of Climate*, *31*(7), 2889–2906. https://doi.org/10.1175/JCLI-D-17-0444.1

Stouffer, R., Hegerl, G., & Tett, S. (2000). A comparison of surface air temperature variability in three 1000-yr coupled ocean-atmosphere model integrations. *Journal of Climate*, *13*, 513–537.

Stouffer, R., Manabe, S., & Vinnikov, K. (1994). Model assessment of the role of natural variability in recent global warming. *Nature*, *367*(6464), 634–636. https://doi.org/10.1038/367634a0

Stouffer, R. J., & Wetherald, R. T. (2007). Changes of variability in response to increasing greenhouse gases. Part I: Temperature. *Journal of Climate*, *20*(21), 5455–5467. https://doi.org/10.1175/2007JCLI1384.1

Tardif, R., G. Hakim, W. Perkins, K. Horlick, M. Erb, J. Emile-Geay, et al. (2019): Last Millennium Reanalysis with an expanded proxy database and seasonal proxy modeling, Clim. Past Discuss., https://doi.org/10.5194/cp-2018-120.

Taylor, K. E., Stouffer, R. J., & Meehl, G. A. (2012). An overview of CMIP5 and the experiment design. *Bulletin of the American Meteorological Society*, *93*(4), 485–498. https://doi.org/10.1175/BAMS-D-11-00094.1

Thomson, D. (1982). Spectrum estimation and harmonic analysis. *Proceedings of the IEEE*, *70*(9), 1055–1096. https://doi.org/10.1109/PROC.1982.12433

Trenberth, K. E., Branstator, G. W., Karoly, D., Kumar, A., Lau, N., & Ropelewski, C. (1998). Progress during TOGA in understanding and modeling global teleconnections associated with tropical sea surface temperatures. *Journal of Geophysical Research*, *103*(C7), 14,291–14,324. https://doi.org/10.1029/97JC01444

Trenberth, K. E., & Fasullo, J. T. (2013). An apparent hiatus in global warming? *Earth Future*, *1*(1), 19–32. https://doi.org/10.1002/2013EF000165

Watanabe, M., Shiogama, H., Tatebe, H., Hayashi, M., Ishii, M., & Kimoto, M. (2014). Contribution of natural decadal variability to global warming acceleration and hiatus. *Nature Climate Change*, *4*(10), 893–897. https://doi.org/10.1038/nclimate2355

Wills, R. C., Armour, K. C., Battisti, D. S., & Hartmann, D. L. (2019). Ocean–atmosphere dynamical coupling fundamental to the Atlantic Multidecadal Oscillation. *Journal of Climate*, *32*(1), 251–272. https://doi.org/10.1175/JCLI-D-18-0269.1

Wills, R. C., Schneider, T., Wallace, J. M., Battisti, D. S., & Hartmann, D. L. (2018). Disentangling global warming, multidecadal variability, and El Niño in Pacific temperatures. *Geophysical Research Letters*, *45*, 2487–2496. https://doi.org/10.1002/2017GL076327

Xie, S., Kosaka, Y., & Okumura, Y. M. (2016). Distinct energy budgets for anthropogenic and natural changes during global warming hiatus. *Nature Geoscience*, *9*, 29–33.

Zhang, Y., Wallace, J. M., & Battisti, D. S. (1997). ENSO-like interdecadal variability: 1900–93. *Journal of Climate*, *10*(5), 1004–1020. https://doi.org/10.1175/1520-0442(1997)010<1004:ELIV>2.0.CO;2